Article

Lanthanide cerium(III) complex with deep-red emission beyond 700 nm

Jiayin Zheng, Haodi Niu, Ruoyao Guo, Huanyu Liu, Yujia Li, Wen Lu, Tianming Zhong, Zuqiang Bian [ID] & Zhiwei Liu [ID] [✉]

Luminescent cerium(III) compounds with $5d$-$4f$ transition have received extensive interest in phosphor, photocatalysis, and electroluminescence. Due to the high vacuum $5d$ energy level, Ce(III) compounds with emission from ultraviolet to yellow region have been well developed, while orange to deep-red emissions are scarce. In this work, we develop a series of molecular Ce(III) complexes with red to deep-red emission by using S-coordinating dithiobiuret ligands, providing new insights into long-wavelength Ce(III) emitters. The longest emission maxima are extended to 725 nm with a photoluminescence quantum efficiency of 31%. Furthermore, it is found that tuning on the steric hindrance yields both mononuclear and dinuclear Ce(III) complexes with different emission colors, as well as different conversion behaviors between the two structures in toluene solution. This work not only shows the great potential of S-coordinating ligands in achieving deep-red Ce(III) emitters, but also demonstrates interesting coordination chemistry of molecular Ce(III) complexes.

Cerium, as a member of the lanthanide elements, has the highest crust abundance among the lanthanide series[1]. Among the various properties of cerium, trivalent cerium (Ce(III)) exhibits unique optical properties in the field of luminescence[2,3] with the radiative transition from $5d^1$ to $4f^1$. Owing to the adjustability of the energy level of $5d$ orbitals and parity-allowed d-f transition mechanism, numerous Ce(III) emitters with tunable emission and short excited decay lifetimes in a nanosecond scale have been reported[4–8]. Without the drag of the intermediate level between the $5d$ and $4f$ state, Ce(III) emitters usually display pretty high photoluminescence quantum yields (PLQYs, Φ_{PL}). According to the above advantages, luminescent Ce(III) compounds have been applied to lighting, photocatalysis[8,9], inkjet printing[10], and electroluminescence devices[5,11–13] with vigorous vitality.

Restricted by the rather high vacuum $5d$ energy level of Ce(III) (6.35 eV[14,15]), most luminescent Ce(III) compounds emit light with high energy from ultraviolet to yellow[12,16–18]. Even in inorganic Ce(III) phosphors that have been extensively studied, orange-red emissions are not common, and the highest PLQY is 45%[19]. Molecular Ce(III) complexes, as a new class of Ce(III) emitters[5,6,9,11,12,20–26], have gradually gained attention in recent years due to well-defined molecular structures, good solubility in organic solvents, and clear structure-activity relationships. As for now, Ce(III) complexes with longer wavelength emission are still rare, as the molecular design requires ligands with even stronger covalence and calls for strong donor ligands like cyclopentadienyl[18,27,28] and pyrazolate[29,30], and the related research is difficult and rare. In 2018, Wickleder et al. reported a yellow-emitting Ce(III) complex $[Ce(Cp^{tBu2})_2(\mu\text{-}Cl)]_2$ with photoluminescence (PL) maxima of 560 nm and a PLQY of 61%[18]. In 2022, Taydakov et al. synthesized orange- and orange-red-emitting Ce(III) coordination polymers based on 2-pyridylpyrazole ligand[29,30]. With stronger bond covalence, the PL maxima of the two complexes redshift to 604 nm and 642 nm with PLQY lower than 1%, respectively. Considering the low cost of cerium element and the potential application of deep-red-emitting materials in photo detectors[31], light-conversion[32,33], and organic light-emitting diodes[34,35], achieving efficient deep-red-emitting Ce(III) complexes through reasonable ligand design is desirable.

In inorganic Ce(III) phosphors, a combination of both nephelauxetic effects on $5d$ centroid shift and crystal-field splitting is

---

Beijing National Laboratory for Molecular Sciences, State Key Laboratory of Rare Earth Materials Chemistry and Applications, College of Chemistry and Molecular Engineering, Peking University, Beijing, China. ✉e-mail: zwliu@pku.edu.cn

extensively applied in the design of materials with different emission wavelengths[36,37]. To fulfill our target, the strategies in inorganic phosphors are worth learning from, that is, both ligand skeletons with coordinating atoms having strong covalence and polarizability to enhance $5d$ centroid shift, and with electron-donating groups to promote ligand-field splitting are in necessity. Inspired by the orange-red-emitting cerium sulfide[38,39], the sulfur atom with high electronegativity and soft-donor properties is selected as the coordination atom to construct molecular Ce(III) complexes with deep-red emission (Fig. 1a).

In this work, with the exploration of strong-donor S-coordinating dithiobiuret ligand, a series of Ce(III) complexes Ce-dtu^{R4} with the formula of Ce$_n$[(N(CSNR$_2$)$_2$]$_{3n}$ ($n = 2$, R = Me, Et; $n = 1$, R = iPr and Cy), N(CSNR$_2$)$^-$ is R group substituted dithiobiuret anion, shortened as dtu^{R4}) emitting red to deep-red light were synthesized. For PL properties, the best two complexes, Ce-dtu^{Me4} and Ce-dtu^{Cy4}, display red- and deep-red-emissions with PL maxima of 640 nm and 725 nm and PLQY of 22% and 31%, respectively (Fig. 1b). For molecular structure, via tuning of the steric hindrance of the ligand, both mononuclear- and dinuclear-type Ce(III) complexes were obtained and the conversion between the two structures has also been elucidated (Fig. 1c). To the best of our knowledge, this work represents new Ce(III) emitter with PL maxima exceeding 700 nm, showing the pioneering result beyond traditional cognition in the luminescence of Ce(III), as well as a unique example jumping out of classical O- or N-coordination systems.

Results
Synthesis and structures
The synthesis routes of the coordination ligands and the corresponding Ce(III) complexes are depicted in Fig. 2. Starting from thiophosgene, the reaction with secondary amine yields the corresponding

thiocarbamoyl chloride. The intermediate was reacted with KSCN and then secondary amine to give symmetrical 1,1,5,5-tetra-substituted dithiobiuret Hdtu^{R4} (R = Me, Et, iPr, and Cy). Hdtu^{Me4} and Hdtu^{Et4} are soluble in acetonitrile (MeCN) and were recrystallized using MeCN, while Hdtu^{iPr4} and Hdtu^{Cy4} were precipitated directly as white solids during the reaction. It's noteworthy that Hdtu^{Et4}, Hdtu^{iPr4} and Hdtu^{Cy4} are not stable enough to be stored even in solid-powder state under inert gas at room temperature, as Brown et al. proposed that dithiobiuret may decompose into carbamoyl isocyanate and corresponding amines upon standing, followed by side reactions of irreversible polymerization[40].

The Ce(III) complexes are denoted as Ce-dtu^{R4} (R = Me, Et, iPr, and Cy). Except for insoluble Ce-dtu^{Me4}, which was synthesized via the acid-base reaction between Hdtu^{Me4} and Ce[N(SiMe$_3$)$_2$]$_3$ in MeCN to afford the pure product, all the other three complexes were synthesized by mixing the stoichiometric Hdtu^{R4} ligand, cerium triflate (Ce(OTf)$_3$), and NaH in tetrahydrofuran (THF) via salt metathesis, followed by recrystallization, because these complexes show great solubility in low-polarity solvents like dichloromethane (DCM) and toluene (PhMe). To further verify the oxidation state of Ce in the prepared samples, X-ray photoelectron spectroscopy (XPS) was conducted for solid-powder Ce-dtu^{R4} (R = Me, Et, iPr, and Cy) complexes. As shown in Supplementary Fig. 1, all four complexes exhibit two peaks centered at about 904 eV and 885 eV, respectively, which are attributed to 3d$_{3/2}$ and 3d$_{5/2}$ of Ce(III)[41], indicating the trivalent essence. Upon standing under nitrogen for several months, the four complexes are stable without observable change, while Ce-dtu^{Et4} decomposes slowly to an unidentified orange-pink powder if there is long-term presence of alcohol solvent vapor in the glove box.

Except for the single crystal of Ce-dtu^{Me4} being obtained during the reaction of Ce[N(SiMe$_3$)$_2$]$_3$ and Hdtu^{Me4}, single crystals of Ce-dtu^{R4}
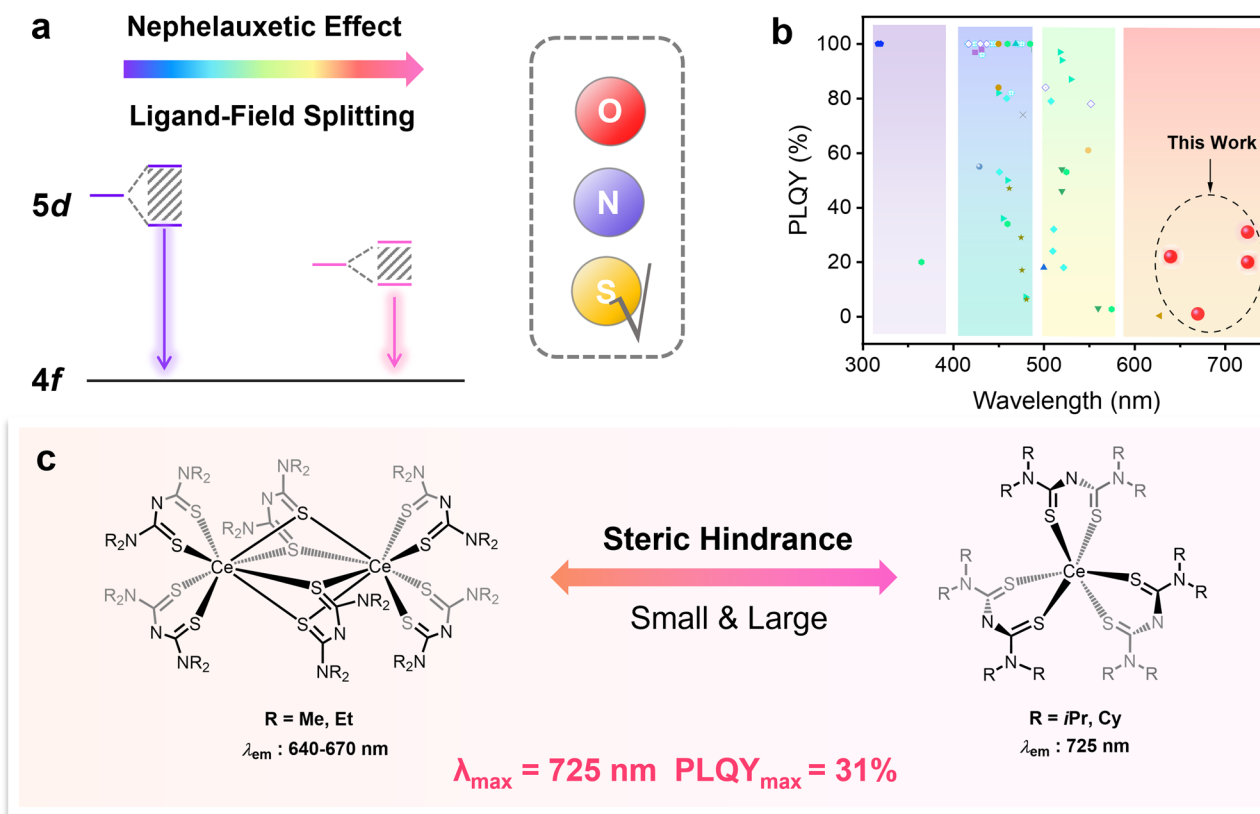

Fig. 1 | Illustration of this work based on red and deep-red-emitting Ce(III) complexes. a Influence of both nephelauxetic effect and ligand-field splitting on $5d$ orbitals and emission energy; **b** Summary of PLQY and PL maxima data of luminescent Ce(III) complexes in literature and this work. **c** Molecular structures of Ce(III) complexes and controllable tuning of mononuclear and dinuclear structures.
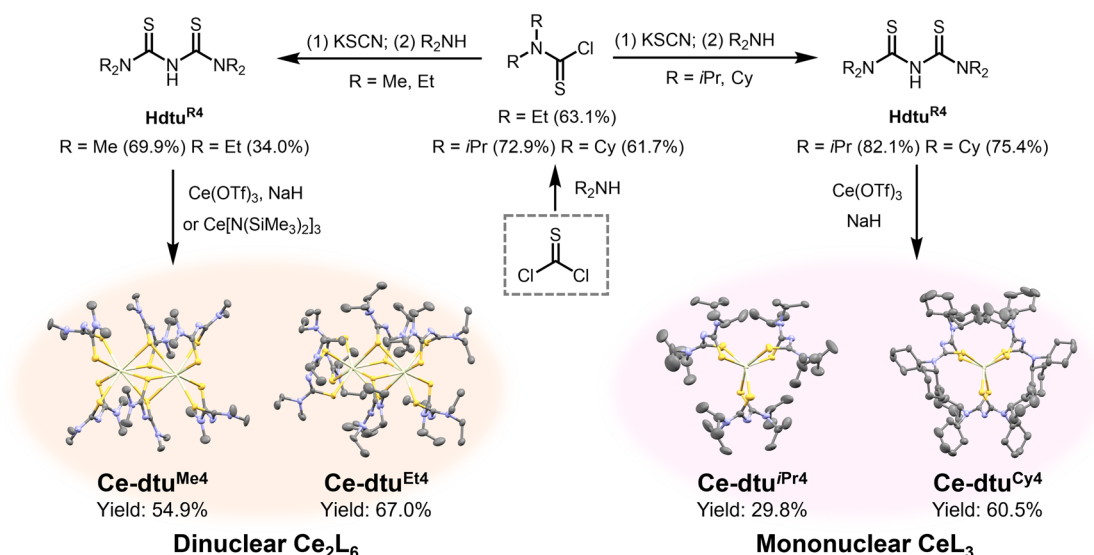
Fig. 2 | Synthetic route of the Hdtu^{R4} ligands (R = Me, Et, *i*Pr, Cy) and synthetic diagram and crystal structures of Ce-dtu^{R4} complexes. Note the data given in parentheses represents the synthesis yield. Note in the molecular structure, the Ce atoms are represented in light-yellow, S in bright yellow, N in blue, C in gray, and H in white.

Table 1 | Structure properties and average Ce-S bond length of Ce-dtu^{R4} complexes (R = Me, Et, *i*Pr, and Cy)

Ce-dtu^{R4}	Nuclearity n	Crystal System	Space Group	Coordination Number	Ave. Ce-S [Å]
R = Me	2	Monoclinic	$P2_1/n$	8	2.968
R = Et	2	Monoclinic	$C2/c$	8	2.969
R = *i*Pr	1	Triclinic	$P\bar{1}$	6	2.835
R = Cy	1	Triclinic	$P\bar{1}$	6	2.836

(R = Et, *i*Pr, and Cy) were obtained by slowly evaporating a mixed solution of the corresponding complex in DCM/THF and *n*-hexane. The molecular structures of these Ce(III) complexes were characterized by single-crystal X-ray diffraction (SXRD), and the coordination geometry of the four complexes can be divided into two classes: dinuclear eight-coordinating and mononuclear six-coordinating. The crystallographic data and coordination bond lengths are shown in Supplementary Table 1 and Supplementary Table 2. The simulated powder X-ray diffraction (PXRD) data using SCXRD data are shown in Supplementary Fig. 2, as the complexes themselves are not stable enough in air to conduct the PXRD experiments. To better understand the molecular structure of the four complexes, the key structure parameters are shown in Table 1. Here, we take Ce-dtu^{Me4} and Ce-dtu^{Cy4} as representatives, considering the smallest and largest steric hindrance across the whole series. In dinuclear Ce-dtu^{Me4}, the crystal belongs to the monoclinic $P2_1/n$ space group. One asymmetric unit contains one Ce(III) center and three dithiobiuret ligands, indicating a completely equivalent coordination environment between the two Ce atoms. Meanwhile, the molecule exhibits C_2-symmetry and coordination geometry of dodecahedron close to tetragonal antiprism, with two different typical Ce-S bond lengths, which are derived from the bonding between Ce(III) and both the terminal ligand (Ave.(Ce-S) = 2.90 Å) and the bridging ligand (Ave.(Ce-S) = 3.04 Å), respectively. In mononuclear Ce-dtu^{Cy4}, the crystal belongs to triclinic $P\bar{1}$ space group. The coordination geometry can be best described as a twisted trigonal prism with C_3-symmetry, and the average Ce-S bond length is 2.84 Å. Compared with dinuclear Ce-dtu^{Me4}, the shorter bond length in Ce-dtu^{Cy4} implies a stronger interaction between the central metal and coordinating atoms.

The structure change of these Ce(III) complexes from dinuclear to mononuclear occurs during the variation of the substituent from ethyl to iso-propyl on the dithiobiuret ligand. As shown in Supplementary Fig. 3, Ce-dtu^{Et4} exhibits a similar but more asymmetric dinuclear structure with Ce-dtu^{Me4}; As for Ce-dtu^{iPr4}, the mononuclear structure is nearly identical to its Ce-dtu^{Cy4} analog. In other words, at least secondary carbon substituents should be attached to N atoms to provide sufficient steric hindrance to obtain mononuclear complexes. In addition, we also tried to synthesize ligands with tertiary carbon substituents and aromatic substituents, such as tert-butyl and phenyl, but the synthesis route didn't work, as either the large steric hindrance or the electron-withdrawing groups may impede the nucleophilic substitution at the first step.

Photophysical properties in solid state

As Ce-dtu^{Me4} is insoluble in common organic solvents, we first studied the photophysical properties of the four Ce-dtu^{R4} complexes in solid-powder state to attain systematic information. The photographs of the complexes under ambient light and 365 nm UV light are shown in Fig. 3a. The PL spectra of dinuclear Ce-dtu^{Me4} (with the smallest steric hindrance ligand) and mononuclear Ce-dtu^{Cy4} (with the largest steric hindrance ligand) were discussed first as representatives. With direct excitation of Ce(III) center via *f-d* absorption (Supplementary Fig. 4), orange-red and deep-red luminescence originating from $5d^1 \rightarrow 4f^1$ (*d-f*) transition can be observed for the two complexes. The PL maxima are 640 nm and 725 nm for Ce-dtu^{Me4} and Ce-dtu^{Cy4} (Fig. 3b), respectively. Considering 4*f* is nearly fixed, the PL maximum difference between the two complexes (85 nm, about 1.83×10^3 cm^{-1}) arises from the different average Ce-S bond lengths and coordination geometries (Ce-dtu^{Me4}: 2.96(8) Å, dodecahedron; Ce-dtu^{Cy4}: 2.83(6) Å, twisted trigonal prism)
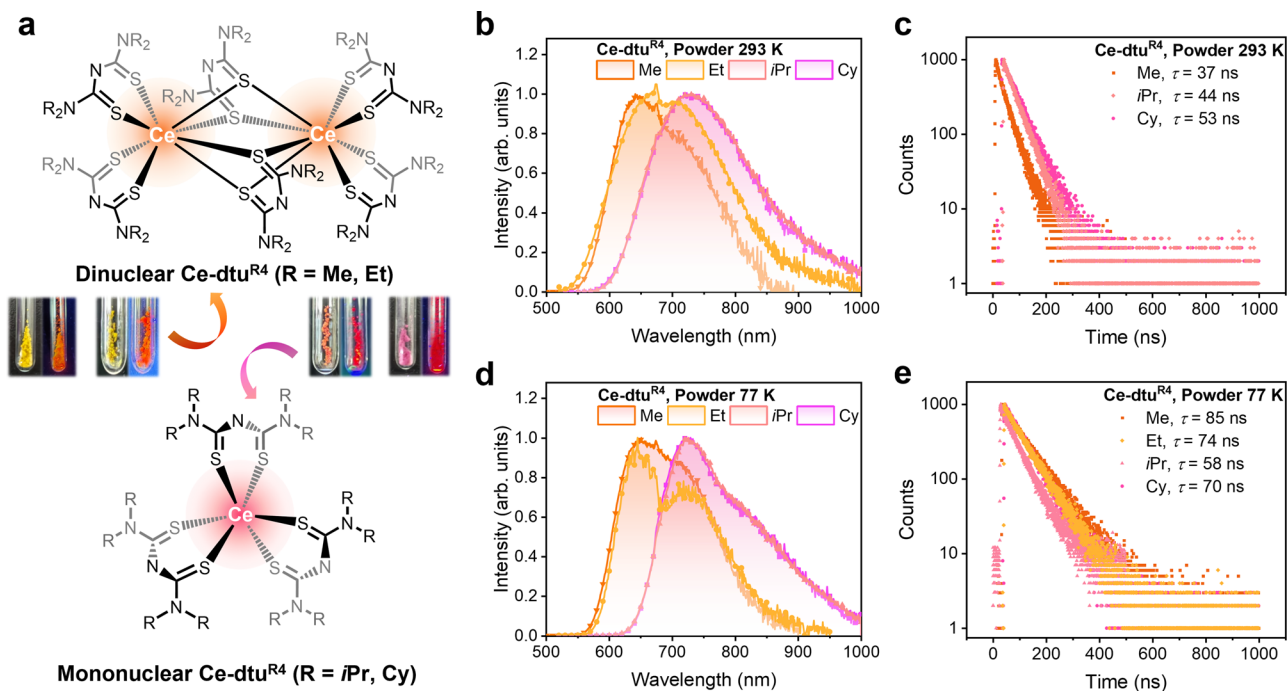
Fig. 3 | PL properties of the four Ce-dtu^{R4} complexes (R = Me, Et, *i*Pr, and Cy) in solid-powder state. a Illustration of the difference in chemical structures and photophysical properties between dinuclear and mononuclear complexes (The images are the four complexes in solid-powder state under ambient light and excitation with 365 nm from R = Me, Et to R = *i*Pr, Cy). **b** Emission spectra of the four complexes and **c** PL decay spectra of the three complexes at 293 K; **d** Emission spectra and **e** PL decay spectra of the four complexes at 77 K. Excitation wavelength: Ce-dtu^{Me4}: 450 nm; Ce-dtu^{Et4}: 500 nm; Ce-dtu^{iPr4}: 490 nm; Ce-dtu^{Cy4}: 500 nm. The excitation source used for PL decay measurement is EPL475.

in the two complexes, which result in distinct impact on 5d centroid shift and/or ligand-field splitting. We can draw on models from inorganic Ce^{3+} phosphors to analyze the impact of 5d centroid shift and ligand-field splitting on the redshift (Supplementary Fig. 5). The centroid shift (ε_C) in Ce-dtu^{Me4} and Ce-dtu^{Cy4} can be roughly compared using the following equation[42] (Eq. 1):

$$\varepsilon_C = N \frac{1.44 \times 10^{17}\alpha_{sp}}{R_{eff}^6} \tag{1}$$

Where N represents the coordination numbers, which are 8 and 6 for Ce-dtu^{Me4} and Ce-dtu^{Cy4}, respectively; α_{sp} is the spectroscopic polarizability related to coordination atoms and can be seen as identical in the two complexes; R_{eff} is treated as the average coordination bond length in the two molecular complexes. Thus, ε_C(Ce-dtu^{Cy4})/ε_C(Ce-dtu^{Me4}) ≈ 0.985, indicating a similar centroid shift on 5d in the two complexes. The ligand-field splitting is directly related to coordination geometry, and the splitting energy in a twisted trigonal prism (Ce-dtu^{Cy4}) is similar to that in an octahedron[42], which is about 1.26 times higher than that in a dodecahedron (Ce-dtu^{Me4})[43]. That is, larger splitting energy instead of centroid shift on 5d finally lowers the lowest 5d energy level in Ce-dtu^{Cy4}, resulting in a redshifted emission maximum to 725 nm. To further elucidate the essence of the d-f transition, Gaussian peak fitting of the PL spectra was conducted. As shown in Supplementary Fig. 6, the emission peak of both complexes can be fitted into double peaks with an energy difference of about 1.8×10^3 cm^{-1}, which corresponds to the transition from the 5d excited state to two 4f sublevels, $^2F_{5/2}$ and $^2F_{7/2}$. Additionally, the excited-state lifetimes in solid-powder state are determined to be 37 ns and 53 ns for Ce-dtu^{Me4} and Ce-dtu^{Cy4} (Fig. 3c), respectively. We are also interested in the luminescence efficiency of these emitters, and their PLQYs are measured to be 22% and 31%. That is, Ce(III) complexes not only show high efficiency with short-wavelength emission as works of literature

reported[4,5,8,23,44], but also exhibit great performance in the red to deep-red region with rational molecule design.

For the other two complexes, Ce-dtu^{Et4} and Ce-dtu^{iPr4}, we will briefly discuss their PL properties. Upon direct f-d excitation, Ce-dtu^{Et4} exhibits weak red emission with PL maxima of 670 nm, and the excited-state lifetime cannot be determined reliably due to the weak luminescence. The Gaussian peak fitting indicates two emission peaks centered at 630 nm and 725 nm (Supplementary Fig. 6), which is similar to the result of Ce-dtu^{Me4}. The more asymmetric molecular structure and higher average atomic displacement parameters (ADP) of sulfur atoms (ADP = 0.0266) compared with its methyl analog (ADP = 0.0245) indicate a lower rigidity and open up more vibrational quenching channels[45,46], which may account for the low efficiency. Ce-dtu^{iPr4} just displays nearly identical PL maxima at 725 nm to its Ce-dtu^{Cy4} analog, suggesting an external alkyl group has little impact on the 5d energy difference. However, the smaller steric hindrance of substituents makes Ce-dtu^{iPr4} easier for Ce(III) centers to interact with the external environment, as well as its slightly lower PLQY of 20% compared with Ce-dtu^{Cy4}, and as discussed before in other literature using guanidinate as anion ligands[23], a more rigid molecular skeleton brings smaller stokes shift and higher efficiency when comparing Ce-dtu^{iPr4} and Ce-dtu^{Cy4}.

At 77 K, the PL spectra of the four complexes in solid-powder state can be well divided into two categories: Dinuclear Ce-dtu^{Me4} and Ce-dtu^{Et4} exhibit orange-red emission, and mononuclear Ce-dtu^{iPr4} and Ce-dtu^{Cy4} show deep-red emission. Between the dinuclear complexes, both share highly resembled PL maxima (Fig. 3d), and a more obvious double-peak emission was observed in Ce-dtu^{Et4}. According to Gaussian peak-fitting, the PL maxima of the 5$d \rightarrow 4f$ ($^2F_{5/2}$) peak are similar in these two complexes (Me: 632 nm; Et: 644 nm) (Supplementary Fig. 7). In addition, the excited-state lifetimes are determined to be 85 ns and 74 ns for the two complexes, respectively. Mononuclear Ce-dtu^{iPr4} and Ce-dtu^{Cy4} display almost the same PL spectra with emission

maxima of 725 nm. Meanwhile, the excited-state lifetimes of the two complexes at 77 K are slightly shorter than those of the dinuclear complexes, with values of 58 ns and 70 ns, respectively (Fig. 3e).

Stability in solution state

The UV-vis absorption spectra (Supplementary Fig. 8) of only three Ce-dtu^{R4} (R = Et, iPr, and Cy) complexes were conducted in PhMe solution since Ce-dtu^{Me4} is insoluble in common organic solvents. The absorption spectra display similar absorption characteristics in these complexes with a strong absorption band ascribed to ligand transition and one weak f-d band (spin- and parity-allowed $4f^1 \rightarrow 5d^1$) of Ce(III). The molar extinction coefficients (ε) of these f-d bands are about $3 \times 10^2\,M^{-1}\cdot cm^{-1}$, as the other literature reported[6,47]. Among them, the f-d bands are within different positions: Absorption of the dinuclear Ce-dtu^{Et4} lies in the range of 420–450 nm, as it is covered by strong ligand absorption; the other two mononuclear complexes exhibit apparent redshifted f-d maxima of 480 nm and 500 nm for Ce-dtu^{iPr4} and Ce-dtu^{Cy4}, respectively.

In addition, to ensure the reliability of the PL data for these complexes in the solution state, we monitored the change of the UV-vis absorption spectra of the three soluble complexes Ce-dtu^{R4} (R = Et, iPr, and Cy) during an 8 h period. As shown in Fig. 4a–c, the intensity of the f-d absorption peaks in all three complexes remained nearly unchanged within 3 h, and exhibits slight degradation after 8 h. The absorbance was selected at the f-d absorption maxima for each complex, and the detailed data are listed in Supplementary Table 3. It's clear to see that Ce-dtu^{Cy4} is the easiest to degrade. Considering the measurements in solution can be conducted within 1 h, the above results indicate the complexes are stable enough for a short-period PL measurement using freshly prepared solutions.

Subsequently, the redox behaviors of these complexes in solution were characterized by studying their cyclic voltammetry (CV) in DCM solutions (10^{-3} M), as the electrolyte [nBu$_4$N][PF$_6$] is not soluble in PhMe. The three complexes exhibit one oxidation peak near 0 V and one at about 0.80 V vs ferrocene redox couple (Fc$^{0/+}$) (Supplementary Fig. 9), indicating their similar redox behaviors. Meanwhile, both oxidations are irreversible for the three complexes according to the cyclic voltammograms. Among the series, Ce-dtu^{Et4} becomes the easiest to oxidize, as the first oxidation peak occurs at about −0.13 V, while those of the other two complexes are 0.16 V (Ce-dtu^{iPr4}) and 0.00 V (Ce-dtu^{Cy4}) vs Fc$^{0/+}$, respectively.

Photophysical properties in solution state

The steady PL spectra of the three complexes in PhMe (10^{-3} M) at 293 K were also measured. With direct f-d excitation (Supplementary Fig. 10a), all three complexes share nearly identical emissions with PL maxima at about 725 nm (Fig. 5a, Supplementary Fig. 11). In addition, the PL spectra remain unchanged even with different excitation

wavelengths (Supplementary Fig. 12), indicating a single luminescence species. It should be noted that Ce-dtu^{iPr4} and Ce-dtu^{Cy4} show similar yet more broadened emission spectra as their solid-powder samples, while Ce-dtu^{Et4} shows a different emission spectrum as its solid-powder sample with a significantly redshifted emission maximum, i.e., from 670 nm to 725 nm. The highly similar PL spectra among the three complexes indicate that they may have the same coordination environment for Ce(III) in solution. As the emission maxima remain identical in Ce-dtu^{iPr4} and Ce-dtu^{Cy4} from solid-powder to solution state, it's plausible to ascribe the existence of mononuclear species of Ce-dtu^{Et4} in PhMe solution too. ^{1}H nuclear magnetic resonance (NMR) spectra of the three complexes in deuterated toluene (tol-d_8) were measured. Besides the peaks arising from the residual solvents in the glovebox (Supplementary Fig. 13), all three complexes show only one group of signals for the corresponding alkyl group (Supplementary Figs. 14–16), indicating that the complex is highly symmetric or undergoes rapid ligand exchange. Furthermore, diffusion ordered NMR spectroscopy (DOSY) is conducted in tol-d_8 to derive the hydrodynamic radius (r_H) of the three complexes, thereby determining the mononuclear nature. As shown in Supplementary Figs. 17–19, the paramagnetism of Ce(III) brings difficulty for distinguishing specific peaks in the NMR spectra, while the self-diffusion coefficient (D_t) can be obtained after the DOSY transform. Thus, the values of r_H were calculated using the Stokes-Einstein Equation (Eq. 2):

$$D_t = \frac{k_B T}{6\pi\eta r_H} \tag{2}$$

Where k_B and T represent the Boltzmann constant and temperature, respectively; η is the viscosity of the deuterated solvent at measuring temperature (0.554 mPa·s for PhMe at 298 K[48,49]). Thus, the r_H are determined to be 5.60 Å, 6,31 Å, and 7.89 Å for Ce-dtu^{Et4}, Ce-dtu^{iPr4}, and Ce-dtu^{Cy4}, respectively. Compared with the results obtained from crystal structure (9.61 Å, 7.63 Å, and 9.03 Å determined by the distance from the center of gravity to the farthest atom), the obvious radius difference between Ce-dtu^{Et4} in solution and crystal (dinuclear structure), as well as the almost identical values of Ce-dtu^{Et4} and Ce-dtu^{iPr4} in solution strongly support the mononuclear structure of Ce-dtu^{Et4} in PhMe solution (Fig. 5b, c), as ethyl and iso-propyl contribute similarly to the radius. That is to say, Ce-dtu^{Et4} experienced a chemical structure conversion from dinuclear to mononuclear when dissolved in PhMe, and the 725 nm emission in solution originates from the mononuclear structure species.

The excited-state lifetimes of these complexes in PhMe (10^{-3} M) at 293 K are determined to be 3.3 ns, 51 ns, and 60 ns for Ce-dtu^{Et4}, Ce-dtu^{iPr4}, and Ce-dtu^{Cy4} (Supplementary Fig. 10b), respectively. The scale in tens of nanoseconds with mono-exponential decay behavior reveals the d-f transition essence of the Ce(III) emitters in PhMe solution. We are also interested in the luminescence efficiency of these deep-red
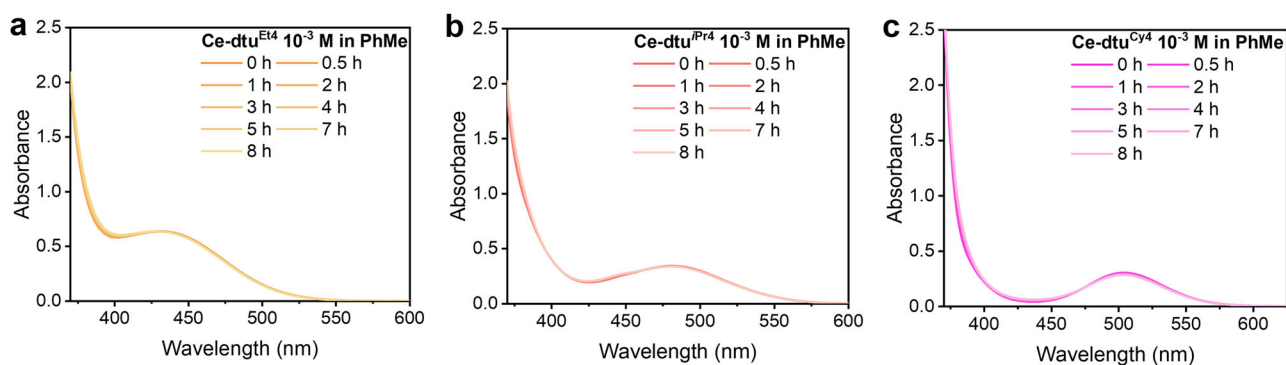
Fig. 4 | Time-dependent UV-vis absorption spectra of Ce-dtu^{R4} (R = Et, iPr, and Cy) in PhMe (10^{-3} M under a N$_2$ atmosphere). a Ce-dtu^{Et4}; **b** Ce-dtu^{iPr4}; **c** Ce-dtu^{Cy4}. PhMe: toluene.
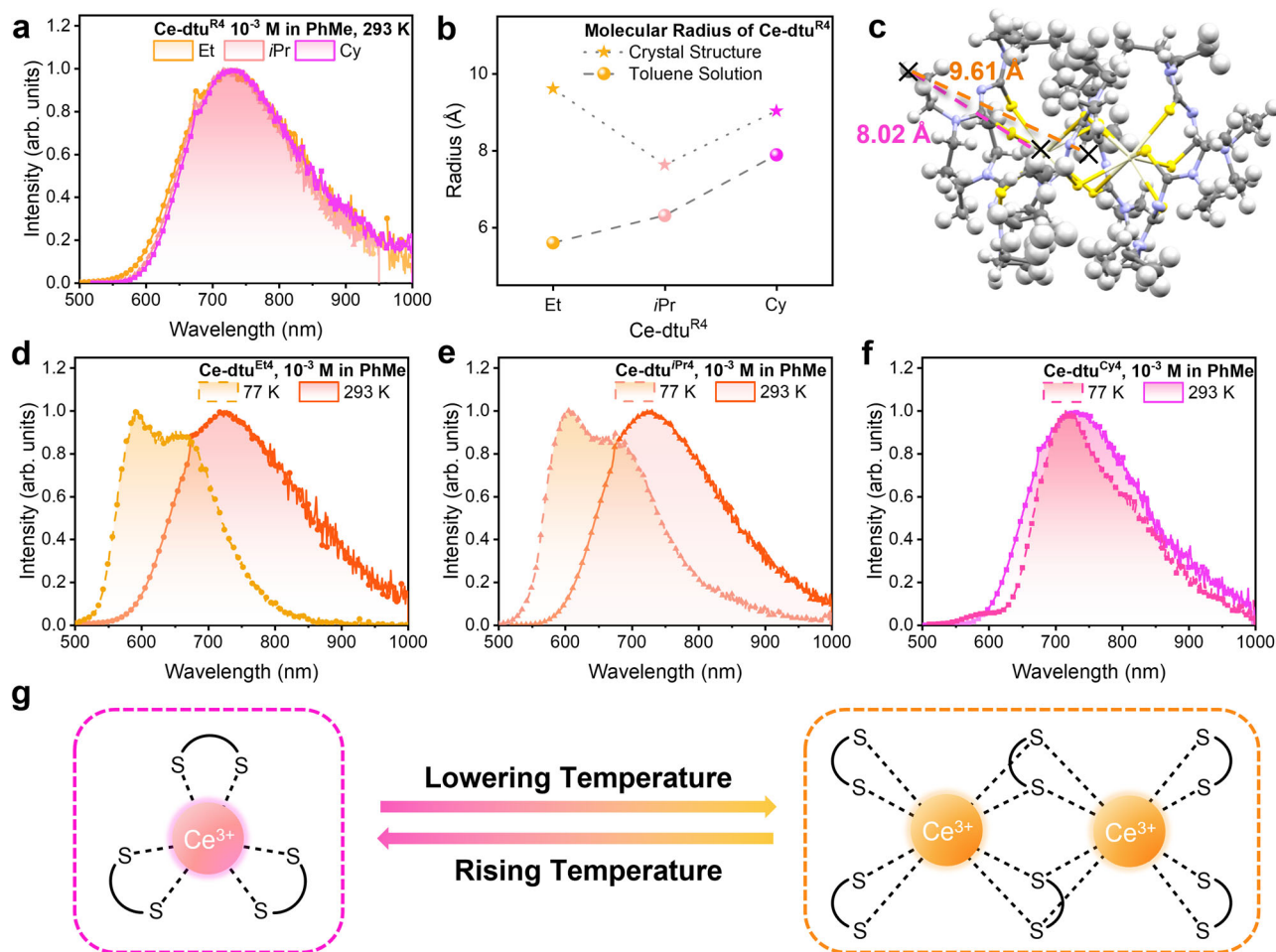
Fig. 5 | PL properties and proposed chemical structure conversion of the three Ce-dtu^{R4} (R = Et, *i*Pr, and Cy) complexes in PhMe solution (10^{-3} M) between 293 K and 77 K. a Emission spectra in PhMe solution at 293 K. **b** Molecular radius of the three complexes obtained from the crystal structure and DOSY experiment. **c** Schematic diagram of the molecular radius of Ce-dtu^{Et4} corresponding to mononuclear and dinuclear structures in the crystal structure (The radius of mononuclear Ce-dtu^{Et4} is estimated by the distance from the farthest point to the Ce(III) center). Emission spectra of **d** Ce-dtu^{Et4}, **e** Ce-dtu^{iPr4}, and **f** Ce-dtu^{Cy4} in PhMe solution at 77 K and 293 K under 350 nm excitation. **g** Illustration of the difference in photophysical properties of Ce-dtu^{R4} in PhMe solution via mononuclear-dinuclear conversion. DOSY: diffusion-ordered NMR spectroscopy. PhMe: toluene.

emitters in PhMe solution, and the PLQYs of Ce-dtu^{Et4}, Ce-dtu^{iPr4}, and Ce-dtu^{Cy4} are measured to be 1%, 17%, and 27%, slightly lower than the values in solid-powder state. As a supplement, the radiative decay rate (k_r) and the non-radiative decay rate (k_{nr}) could also be derived using the equations $k_r = \Phi_{PL}/\tau$ and $1/\tau = k_r + k_{nr}$, and the photophysical data are summarized and listed in Table 2 for comparison in both solid-powder and solution states. It's clear to see a significantly faster k_{nr} in Ce-dtu^{Et4} compared with the other two complexes in PhMe solutions, which may be due to the ethyl group with less steric hindrance and less rigidity, leading to an easier access for the solvent to interact with the Ce(III) center.

We further measured the PL spectra of the three complexes in PhMe solution at 77 K for deeper insight. For Ce-dtu^{Et4}, a large blueshift compared to the spectrum at 293 K is observed, showing a PL maximum at 600 nm under 350 nm excitation (Fig. 5d). The mono-exponential decay with an excited-state lifetime of 103 ns supports the *d-f* essence of the emission band. Different excitation wavelengths, such as 365 nm, 425 nm, and 490 nm, were also used, but no emission band centered at 725 nm was observed (Supplementary Fig. 20). In this context, considering the mono- and di-nuclear structures could be tuned by the steric hindrance of the alkyl group, we suggest the coordination structure of Ce-dtu^{Et4} in PhMe solution is temperature-

dependent as well, and low temperature could stabilize the dinuclear structure to induce high energy emission (600 nm).

The low-temperature behavior of the other two complexes, Ce-dtu^{iPr4} and Ce-dtu^{Cy4}, differs from dtu^{Et4}. Under 350 nm excitation, Ce-dtu^{iPr4} exhibits similar PL spectra with Ce-dtu^{Et4}, while a difference lies in the tail at 800–1000 nm in the spectrum (Fig. 5e). Under 500 nm excitation, the 725 nm emission emerged as the main component (Supplementary Fig. 21), which indicates the existence of two luminescence species (600 nm and 725 nm) under the experiment condition and explains that the aforementioned tail is the 725 nm emission. Compared to the excitation-independent emission of Ce-dtu^{Et4} centered at 600 nm, the excitation-dependent emission of Ce-dtu^{iPr4} indicates the concurrent existence of mononuclear and dinuclear structures at 77 K. Subsequently, for Ce-dtu^{Cy4} with larger steric hindrance, the 600 nm emission just manifests as a small band, and 725 nm emission becomes dominant under 350 nm excitation (Fig. 5f), implying the fact that Ce-dtu^{Cy4} is more difficult to become a dinuclear structure. Furthermore, monitoring of both emissions at 600 nm and 725 nm yields two different excitation spectra and excited-state life-times as well (Supplementary Fig. 22), which strongly supports the existence of two luminescent species in the PhMe solutions of both Ce-dtu^{iPr4} and Ce-dtu^{Cy4} at 77 K. Therefore, through the complexes from

Table 2 | Photophysical properties of Ce-dtu^{R4} (R = Me, Et, *i*Pr, and Cy) complexes in solid-powder state and PhMe solution (10^{-3}M) at 293 K

Ce-dtu^{R4}	State	PL Maxima[b] [nm]	PLQY [%]	τ[d] [ns]	FWHMs [nm] (10^3 cm^{-1})	k_r[d] [10^6 s^{-1}]	k_{nr}[d] [10^6 s^{-1}]
R = Me[a]	Powder	640 (639, 738)	22	37	184 (4.08)	5.9	21
R = Et[c]	Powder	670 (630, 725)	-	-	201 (4.22)	-	-
	PhMe solution	725 (684, 758)	1	3.3	244 (3.78)	3	300
R = *i*Pr	Powder	725 (702, 780)	20	44	203 (3.68)	4.5	18
	PhMe solution	725 (688, 762)	17	43	197 (3.62)	4.0	19
R = Cy	Powder	725 (710, 792)	31	53	190 (3.46)	5.8	13
	PhMe solution	725 (695, 769)	27	57	201 (3.63)	4.7	13

a: Ce-dtu^{Me4} is insoluble in PhMe.

b: The values in parentheses represent the emission maxima from 5d to two 4f sublevels ($^2F_{5/2}$ and $^2F_{7/2}$) obtained from Gaussian peak fitting.

c: The emission of solid-powder Ce-dtu^{Et4} is too weak; thus, the PLQY and the excited-state lifetime cannot be determined explicitly.

d: τ, k_r, and k_{nr} represent the excited-state lifetime, radiative decay rate, and non-radiative decay rate, respectively.

Ce-dtu^{Et4} to Ce-dtu^{iPr4} and Ce-dtu^{Cy4}, a gradually increased steric hindrance yields complete to lower 600 nm component (i.e. dinuclear structure component), indicating the structure conversion is also temperature-dependent in solution (Fig. 5g).

Discussion

In summary, deep-red Ce(III) emitters with PL maxima exceeding 700 nm has been synthesized and characterized using S-coordinating dithiobiuret ligands. By applying different steric hindrances, dinuclear and mononuclear Ce(III) complexes were obtained with red and deep-red emissions, respectively, due mainly to different splitting energies rather than the centroid shift of the 5d orbital. Among them, the best two complexes, dinuclear Ce-dtu^{Me4} and mononuclear Ce-dtu^{Cy4}, exhibit red emission centered at 640 nm and deep-red emission centered at 725 nm with PLQY of 22% and 31%, respectively. The exciting result exceeds the common understanding of the emission color of Ce(III) compounds, which may raise new attention in designing red to near-infrared d-f emitters. Furthermore, temperature-dependent PL spectra suggest different chemical structure conversions between monomer and dimer in these Ce(III) complexes, revealing interesting coordination chemistry among these unique complexes. This work not only demonstrates the pioneering use of S-coordinating ligands in lanthanide Ce(III) complexes, but also reveals the huge potential of Ce(III) to construct highly efficient deep-red, even near-infrared emitters.

Methods

General information

All synthesis experiments were performed under a nitrogen atmosphere. All chemical reagents used in the synthesis process were commercially available and were used as received unless otherwise mentioned. The synthesis and purification of Ce(III) complexes were carried out in a glove box. Ce(OTf)$_3$ was dried under vacuum at 180 °C prior to use. The solvents used to synthesize the complexes were specially treated: THF, PhMe, tol-d_8, and n-hexane were dried over sodium/benzophenone and freshly distilled under an argon atmosphere; DCM and MeCN were dried over calcium hydride and freshly distilled under an argon atmosphere. Powder-state NaH was prepared by washing commercially available 60% NaH with n-hexane (3 × 20 mL) in a glovebox. All glasswares were oven-dried at 120 °C for at least 1 h before use.

^{1}H NMR spectra were recorded on a Bruker-400 MHz NMR spectrometer. Tetramethylsilane (TMS) was used as an internal reference for the chemical shift correction, where δ(TMS) equals 0. The ^{13}C NMR spectra and DOSY NMR spectra were recorded on a Bruker-500 MHz NMR spectrometer. Electrospray ionization mass spectra (ESI-MS) were performed in negative ion mode on a Bruker Apex IV Fourier

transform ion cyclotron resonance mass spectrometer. The infrared spectrum (IR) of the product (KBr pellets) was recorded using a Fourier transform infrared spectrometer (Nicolet Is50, ThermoFisher) in the range of 400–4000 cm^{-1} the results are shown in Supplementary Figs. 23–24. X-ray photoelectron spectroscopy was performed on an AXIS Supra X-ray photoelectron spectrometer.

Synthesis of thiocarbamoyl chloride

Synthesis of Et$_2$NC(S)Cl. To an orange solution of thiophosgene (11.50 g, 0.100 mol) in 50 mL THF in an ice-salt bath, Et$_2$NH (14.63 g, 0.200 mol) in 50 mL THF was added dropwise over 1 h, the amine hydrochloride precipitated immediately, and the mixture became cloudy. After the addition, the mixture was stirred at room temperature for a further 45 min. The amine hydrochloride was filtered off and washed with 20 mL THF. The brown filtrate was combined, and the solvent was removed in vacuo to afford a brown solid, which was washed with n-hexane (3 × 20 mL) to give pale-brown to off-white crystalline powder. Yield: 9.56 g (63.1%). ^{1}H NMR (400 MHz, CDCl$_3$): δ 3.87 (dq, J = 61.6, 7.1 Hz, 4H), 1.33 (td, J = 7.1, 2.8 Hz, 6H); ^{13}C{^{1}H} NMR (126 MHz, CDCl$_3$): δ 174.12, 50.30 (d, J = 36.0 Hz), 12.98, 10.95; IR (v, KBr pellet): 2977, 2935, 2856, 2820, 2038, 1668, 1505, 1457, 1443, 1425, 1354, 1275, 1199, 1147, 1094, 1067 cm^{-1}.

Synthesis of iPr$_2$NC(S)Cl. A similar procedure of synthesis of Et$_2$NC(S)Cl was used with thiophosgene (8.70 g, 75.7 mmol) in 70 mL THF and iPr$_2$NH (15.20 g, 150 mmol) in 50 mL THF to give pale-brown crystalline powder. Yield: 9.82 g (72.9%). ^{1}H NMR (400 MHz, CDCl$_3$): δ 3.47–3.33 (m, J = 6.4 Hz, 2H), 1.50 (d, J = 6.5 Hz, 12H); ^{13}C{^{1}H} NMR (126 MHz, CDCl$_3$): δ 47.50, 19.28; IR (v, KBr pellet): 2973, 2934, 2835, 2759, 2721, 1668, 1624, 1464, 1399, 1378, 1320, 1275, 1187, 1141, 1117, 1026 cm^{-1}.

Synthesis of Cy$_2$NC(S)Cl. A similar procedure of synthesis of Et$_2$NC(S)Cl was used with thiophosgene (5.75 g, 50.0 mmol) in 50 mL THF and Cy$_2$NH (18.1 g, 100 mmol) in 50 mL THF to give off-white crystalline powder. Yield: 8.02 g (61.7%). ^{1}H NMR (400 MHz, CDCl$_3$): δ 2.55 (s, 2H), 1.75 (d, J = 72.6 Hz, 10H), 1.48–1.25 (m, 6H), 1.16 (q, J = 13.0 Hz, 4H); ^{13}C{^{1}H} NMR (126 MHz, CDCl$_3$): δ 62.70, 30.79, 29.36 (d, J = 15.7 Hz), 26.37 (d, J = 41.0 Hz), 24.96 (d, J = 40.0 Hz); IR (v, KBr pellet): 2932, 2854, 1476, 1441, 1371, 1346, 1312, 1268, 1242, 1162, 1090, 997, 949, 898, 871 cm^{-1}.

Synthesis of 1,1,5,5-tetra-substituted dithiobiuret ligand

Synthesis of [Me$_2$NC(S)]$_2$NH (Hdtu^{Me4}). To a mixture of Me$_2$C(S)Cl (3.78 g, 30.0 mmol) and KSCN (2.95 g, 30.3 mmol) was added 60 mL MeCN. The reaction mixture was heated and refluxed for 3 h. After cooling down, the yellow mixture was filtered. The filtered KCl was washed with 10 mL MeCN, and the filtrate was combined. Then 2 M

Me_2NH in THF (16.0 mL, 32.0 mmol) was added to the yellow filtrate of $Me_2NC(S)NCS$, and the solution was stirred overnight. The solvent was removed in vacuo, and the residue was washed with Et_2O (3 × 20 mL) and PhMe (20 mL) to afford a pale-brown solid. Yield: 4.01 g (69.9%). ^1H NMR (400 MHz, $CDCl_3$): δ 3.35 (m, 12H); $^{13}C\{^1H\}$ NMR (126 MHz, $CDCl_3$): δ 181.44, 43.05; ESI-MS (m/z) [M-H]⁻ calcd. for $C_6H_{12}N_3S_2$, 190.05; found, 190.05; IR (v, KBr pellet): 3218, 2930, 1546, 1466, 1386, 1289, 1261, 1219, 1153, 1105, 742 cm⁻¹.

Synthesis of $[Et_2NC(S)]_2NH$ (Hdtu^{Et4}). A similar procedure of synthesis of Hdtu^{Me4} was used with $Et_2C(S)Cl$ (4.55 g, 30.0 mmol) and KSCN (2.91 g, 30.0 mmol) in 50 mL MeCN. Et_2NH (4.20 g, 57.4 mmol) was added to the yellow filtrate of $Et_2NC(S)NCS$, and the reaction was stirred overnight. The solvent was removed in vacuo, and the obtained brown solid was washed with a small amount of MeCN (3 × 1 mL) to afford an off-white powder. The filtrate can be further concentrated to yield more crystalline products. Yield: 2.52 g (34.0%). ^1H NMR (400 MHz, $CDCl_3$): δ 4.04–3.49 (m, 8H), 1.28 (t, J = 7.2 Hz, 12H); $^{13}C\{^1H\}$ NMR (126 MHz, $CDCl_3$): δ 180.01, 46.57, 12.56; ESI-MS (m/z) [M-H]⁻ calcd. for $C_{10}H_{20}N_3S_2$, 246.11; found, 246.11; IR (v, KBr pellet): 3203, 2974, 2931, 2871, 1533, 1503, 1430, 1346, 1266, 1228,1192, 1123, 1073, 1011 cm⁻¹.

Synthesis of $[iPr_2NC(S)]_2NH$ (Hdtu^{iPr4}). A similar procedure of synthesis of Hdtu^{Me4} was used with $iPr_2C(S)Cl$ (3.49 g, 20.0 mmol) and KSCN (1.95 g, 20.0 mmol) in 50 mL MeCN. iPr_2NH (4.05 g, 40.0 mmol) was added to the yellow filtrate of $iPr_2NC(S)NCS$, and white Hdtu^{iPr4} precipitated with stirring. The mixture was filtered after stirring overnight, and the obtained solid was washed with MeCN (3 × 5 mL) to afford an off-white powder. The filtrate can be further concentrated to yield more crystalline products. Yield: 4.99 g (82.1%). ^1H NMR (400 MHz, $CDCl_3$): δ 2.92 (hept, J = 6.3 Hz, 4H), 1.05 (d, J = 6.2 Hz, 24H); $^{13}C\{^1H\}$ NMR (126 MHz, $CDCl_3$): δ 45.46, 22.95; ESI-MS (m/z) [M-H]⁻ calcd. for $C_{14}H_{28}N_3S_2$, 302.17; found, 302.17; IR (v, KBr pellet): 2970, 2931, 2870, 1999, 1569, 1489, 1456, 1369, 1341, 1271, 1250, 1227, 1209, 1147, 1099, 1035 cm⁻¹.

Synthesis of $[Cy_2NC(S)]_2NH$ (Hdtu^{Cy4}). A similar procedure of synthesis of Hdtu^{Me4} was used with $Cy_2C(S)Cl$ (3.90 g, 15.0 mmol) and KSCN (1.46 g, 15.0 mmol) in 50 mL MeCN. Cy_2NH (3.62 g, 20.0 mmol) was added to the yellow filtrate of $Cy_2NC(S)NCS$, and white Hdtu^{Cy4} precipitated with stirring. The mixture was filtered after stirring overnight, and the obtained solid was washed with MeCN (3 × 15 mL) to afford an off-white powder. Yield: 5.25 g (75.4%). ^1H NMR (400 MHz, $CDCl_3$): δ 2.55 (tt, J = 10.6, 3.8 Hz, 4H), 1.95–1.54 (m, 16H), 1.48–0.90 (m, 24H); $^{13}C\{^1H\}$ NMR (126 MHz, $CDCl_3$): δ 53.12, 34.23, 26.17, 25.31; ESI-MS (m/z) [M-H]⁻ calcd. for $C_{26}H_{44}N_3S_2$, 462.30; found, 462.30; IR (v, KBr pellet): 2930, 2851, 1587, 1464, 1450, 1367, 1343, 1271, 1213, 1180, 1123, 1093, 992, 894 cm⁻¹.

Synthesis of the cerium complex
Synthesis of $Ce_2[N(C(S)NMe_2)_2]_6$. Hdtu^{Me4} (286 mg, 1.50 mmol) was dissolved in 15 mL MeCN and added to the solution of $Ce[N(SiMe_3)_2]_3$ (330 mg, 0.53 mmol) in 15 mL MeCN. Orange-yellow powder precipitated immediately. The reaction mixture was stirred for 1 day at room temperature and then filtered. The filtered solid was washed with MeCN (3 × 10 mL) and THF (2 × 10 mL) to give an orange-yellow solid. Yield: 267 mg (54.9%) for powder sample. The single crystals were obtained by slowly diffusion the MeCN solution of $Ce[N(SiMe_3)_2]_3$ into the MeCN solution of Hdtu^{Me4}. Analysis (calcd., found for $C_{36}H_{72}N_{18}S_{12}Ce_2 + 0.5C_4H_8O$, M = 1458.10 g/mol): C (31.30, 31.13), H (5.25, 5.05), N (17.29, 17.32).

Synthesis of $Ce_2[N(C(S)NEt_2)_2]_6$. To the mixture of Hdtu^{Et4} (741 mg, 3.00 mmol) and NaH (72 mg, 1.50 mmol) was added 15 mL THF to prepare the ligand salt in situ. Then the yellow ligand slurry was added to a slurry of $Ce(OTf)_3$ (587 mg, 1.00 mmol) in 15 mL THF. The colorless slurry turned to orange-yellow immediately, and the reaction mixture was stirred for 1 day at room temperature. The solvent was removed in vacuo, and the residue was extracted with 25 mL PhMe and filtered. The solvent of the orange-red filtrate was removed to give an orange solid. Yield: 589 mg (67.0%) for powder sample. The single crystals were obtained by slowly evaporating the mixed solution of THF and n-hexane. Analysis (calcd., found for $C_{60}H_{120}N_{18}S_{12}Ce_2$, M = 1758.68 g/mol), C (40.97, 40.74), H (6.88, 6.81), N (14.34, 14.05).

Synthesis of $Ce[N(C(S)NiPr_2)_2]_3$. To the mixture of Hdtu^{iPr4} (910 mg, 3.00 mmol) and NaH (72 mg, 3.00 mmol) was added 15 mL THF to prepare ligand salt in situ. Then the ligand slurry was added to a slurry of $Ce(OTf)_3$ (587 mg, 1.00 mmol) in 15 mL THF. The colorless slurry turned orange immediately, and the reaction mixture was stirred for 1 day at room temperature. The solvent was removed in vacuo, and the residue was extracted with 25 mL n-hexane and filtered. The solvent of the orange-red filtrate was removed again to give a pink solid, which is no longer easily soluble in n-hexane. The solid was washed with n-hexane (3 × 10 mL) to give a coral-red to peach-colored powder. Yield: 312 mg (29.8%) for powder sample. The single crystals were obtained by slowly evaporating the mixed solution of DCM and n-hexane. Analysis (calcd., found for $C_{42}H_{84}N_9S_6Ce$, M = 1047.69 g/mol), C (48.15, 48.26), H (8.08, 8.07), N (12.04, 11.90).

Synthesis of $Ce[N(C(S)NCy_2)_2]_3$. A similar procedure to above was used with Hdtu^{Cy4} (696 mg, 1.50 mmol), NaH (54 mg, 2.25 mmol), and $Ce(OTf)_3$ (293 mg, 0.50 mmol). The residue from THF was extracted with 25 mL PhMe and filtered. The solvent of the orange-red filtrate was then removed in vacuo. The residue was washed with a 10 mL mixed solution of DCM and n-hexane (1:4 in volume ratio) to give a magenta powder. Yield: 475 mg (60.5%) for powder sample. The single crystals were obtained by slowly evaporating the mixed solution of DCM and n-hexane. Analysis (calcd., found for $C_{78}H_{132}N_9S_6Ce + 0.5CH_2Cl_2$, M = 1570.91 g/mol), C (60.01, 60.25), H (8.53, 8.74), N (8.03, 7.49).

Single-crystal X-ray crystallography
The single-crystal X-ray diffraction data were obtained with a Rigaku007HF Saturn CCD Diffractometer utilizing Mo Kα radiation with a wavelength of 0.71073 Å via the CrystalClear software package. All structures were solved by the intrinsic phasing method with SHELXT5 and refined by full-matrix least-squares procedures utilizing SHELXL within the Olex2 crystallographic software package[50]. The PXRD data were simulated using the SCXRD data of the corresponding complexes via the CCDC Mercury software package[51]. The molecular structures of the complexes using ORTEP-style are shown in Supplementary Fig. 25.

Spectral measurements
All the solutions used for measurement were freshly prepared to avoid the influence of degradation. The UV-vis absorption spectra were obtained from a Shimadzu UV-3100 spectrometer. Steady/transient photoluminescence spectra were recorded on an Edinburgh Analytical Instruments FLS980 spectrophotometer equipped with a pulsed laser (Edinburgh Ltd. Co.). The spectral tests of solid-powder complexes at room temperature were carried out by paraffin encapsulation between two quartz plates, and the solutions were protected by capped cuvettes under a N_2 atmosphere. The spectral tests of samples at 77 K were conducted in a quartz NMR tube equipped with caps in a Dewar flask. The photoluminescence quantum yields (PLQYs) were measured by an absolute PLQY measurement system on C9920-02 from Hamamatsu Company.

Cyclic voltammetric measurements
Cyclic voltammetry was performed in the range of −1.8 V to 1.8 V, at 0.1 V/s scan rate in DCM containing 0.1 M [nBu_4N][PF_6] as electrolyte. For internal reference, ferrocene (Fc) was added after scanning the solution of the complex.

Data availability

The main data supporting the findings of this study are shown within the article and its Supplementary Figs. and are provided in the Supplementary Information/Source Data file. The source data underlying Figs. 3–5, Supplementary Figs. 1–2, Supplementary Fig. 4, Supplementary Figs. 8–10, Supplementary Fig. 12, and Supplementary Figs. 20–22 are provided as a Source Data file. Source data are provided with this paper. Crystallography data have been deposited at the Cambridge Crystallographic Data Centre (CCDC) under deposition numbers CCDC 2401372 (Ce-dtu^{Me4}), 2401373 (Ce-dtu^{Et4}), 2401374 (Ce-dtu^{Cy4}), and 2401375 (Ce-dtu^{iPr4}), and are publicly available as of the date of publication. Copies of the data can be obtained free of charge via https://www.ccdc.cam.ac.uk/structures/. All data are available from the corresponding author upon request. Source data are provided with this paper.

References

1. Yaroshevsky, A. A. Abundances of chemical elements in the Earth's crust. *Geochem. Int.* **44**, 48–55 (2006).
2. Wang, L. et al. Review on the electroluminescence study of lanthanide complexes. *Adv. Opt. Mater.* **7**, 1801256 (2019).
3. Gao, S., Cui, Z. & Li, F. Doublet-emissive materials for organic light-emitting diodes: exciton formation and emission processes. *Chem. Soc. Rev.* **52**, 2875–2885 (2023).
4. Fang, P. et al. Delayed doublet emission in a cerium(III) complex. *Angew. Chem. Int. Ed.* **62**, e202302192 (2023).
5. Fang, P. et al. Lanthanide cerium (III) tris (pyrazolyl) borate complexes: efficient blue emitters for doublet organic light-emitting diodes. *ACS Appl. Mater. Inter.* **13**, 45686–45695 (2021).
6. Yan, W. et al. Highly efficient heteroleptic cerium (III) complexes with a substituted pyrazole ancillary ligand and their application in blue organic light-emitting diodes. *Inorg. Chem.* **60**, 18103–18111 (2021).
7. Yan, W. et al. Deep-blue emitting cerium (III) complexes with tris (pyrazolyl) borate and triflate ligand_. *Dalton Trans.* **51**, 3234-3240 (2022).
8. Yin, H., Carroll, P. J., Anna, J. M. & Schelter, E. J. J. J. O. T. A. C. S. Luminescent Ce (III) complexes as stoichiometric and catalytic photoreductants for halogen atom abstraction reactions. *J. Am. Chem. Soc.* **137**, 9234–9237 (2015).
9. Yin, H., Carroll, P. J., Manor, B. C., Anna, J. M. & Schelter, E. J. J. J. O. T. A. C. S. Cerium photosensitizers: structure–function relationships and applications in photocatalytic aryl coupling reactions. *J. Am. Chem. Soc.* **138**, 5984–5993 (2016).
10. Du, H. et al. Electrohydrodynamically printed d–f transition cerium(III) complex. *J. Phys. Chem. Lett.* **15**, 874–879 (2024).
11. Wang, L. et al. Deep-blue organic light-emitting diodes based on a doublet d–f transition cerium (III) complex with 100% exciton utilization efficiency. *Light Sci. Appl* **9**, 1–9 (2020).
12. Zhao, Z. et al. Efficient rare earth cerium (III) complex with nanosecond df emission for blue organic light-emitting diodes. *Natl. Sci. Rev.* **8**, nwaa193 (2020).
13. Fang, P. et al. Lanthanide complexes with *d-f* transition: New emitters for single-emitting-layer white organic light-emitting diodes. *Light Sci. Appl* **12**, 170 (2023).
14. Ueda, J. & Tanabe, S. Review of luminescent properties of Ce^{3+}-doped garnet phosphors: New insight into the effect of crystal and electronic structure. *Opt. Mater. X* **1**, 100018 (2019).
15. Blasse, G. & Bril, A. Investigation of some Ce^{3+}-activated phosphors. *J. Chem. Phys.* **47**, 5139–5145 (2004).
16. Wen, Z. et al. Optimizing energy transfer: suppressing Cs$_2$ZnCl$_4$ self-trapped states and boosting Ce^{3+} ion luminescence efficiency. *Laser Photonics Rev.* **18**, 2400525 (2024).
17. Wang, Q. et al. Ultraviolet emission from cerium-based organic-inorganic hybrid halides and their abnormal anti-thermal quenching behavior. *Adv. Funct. Mater.* **33**, 2303399 (2023).
18. Suta, M. et al. Bright photoluminescence of [{(Cp)$_2$Ce(μ-Cl)}]$_2$: a valuable technique for the determination of the oxidation state of cerium. *Chem. Asian J.* **13**, 1038–1044 (2018).
19. You, S., Li, S., Jia, Y. & Xie, R.-J. Interstitial site engineering for creating unusual red emission in La$_3$Si$_6$N$_{11}$:Ce^{3+}. *Chem. Mater.* **32**, 3631–3640 (2020).
20. Blasse, G., Dirksen, G., Sabbatini, N. & Perathoner, S. J. I. C. A. Photophysics of Ce^{3+} cryptates. *Inorg. Chim. Acta* **133**, 167–173 (1987).
21. Yu, T. et al. Ultraviolet electroluminescence from organic light-emitting diode with cerium (III)–crown ether complex. *Solid·State Electron* **51**, 894–899 (2007).
22. Zheng, X. L. et al. Bright blue-emitting Ce^{3+} complexes with encapsulating polybenzimidazole tripodal ligands as potential electroluminescent devices. *Angew. Chem. Int. Ed.* **46**, 7399–7403 (2007).
23. Qiao, Y. et al. Understanding and controlling the emission brightness and color of molecular cerium luminophores. *J. Am. Chem. Soc.* **140**, 4588–4595 (2018).
24. Yin, H., Carroll, P. J., Anna, J. M. & Schelter, E. J. Luminescent Ce(III) complexes as stoichiometric and catalytic photoreductants for halogen atom abstraction reactions. *J. Am. Chem. Soc.* **137**, 9234–9237 (2015).
25. Guo, R. et al. Complexes of Ce (III) and bis (pyrazolyl) borate ligands: Synthesis, structures, and luminescence properties. *Inorg. Chem.* **61**, 14164–14172 (2022).
26. Fang, P. et al. Delayed doublet emission in a cerium (III) complex. *Angew. Chem. Int. Ed.* **62**, e202302192 (2023).
27. Hazin, P. N., Bruno, J. W. & Brittain, H. G. Luminescence spectra of a series of cerium(III) halides and organometallics. Probes of bonding properties using 4*f*-5*d* excited states. *Organometallics* **6**, 913–918 (1987).
28. Rausch, M. D. et al. Synthetic, X-ray structural and photoluminescence studies on pentamethylcyclopentadienyl derivatives of lanthanum, cerium and praseodymium. *Organometallics* **5**, 1281–1283 (1986).
29. Youssef, H. et al. Red emitting cerium(III) and versatile luminescence chromaticity of 1D-coordination polymers and heterobimetallic Ln/AE pyridylpyrazolate complexes. *Z. Anorg. Allg. Chem.* **648**, e202200295 (2022).
30. Youssef, H., Sedykh, A. E., Becker, J., Taydakov, I. V. & Müller-Buschbaum, K. 3-(2-Pyridyl)pyrazole based luminescent 1D-coordination polymers and polymorphic complexes of various lanthanide chlorides including orange-emitting cerium(III). *Inorganics* **10**, 254 (2022).
31. Chow, P. C. Y. & Someya, T. Organic photodetectors for next-generation wearable electronics. *Adv. Mater.* **32**, 1902045 (2020).
32. Wu, W. et al. Characterization and properties of a Sr$_2$Si$_5$N$_8$:Eu^{2+}-based light-conversion agricultural film. *J. Rare Earths* **38**, 539–545 (2020).
33. Yang, C. et al. Recent advances in light-conversion phosphors for plant growth and strategies for the modulation of photoluminescence properties. *Nanomaterials* **13**, 1715 (2023).
34. Pu, Y. et al. Sulfur-locked multiple resonance emitters for high performance orange-red/deep-red OLEDs. *Nat. Commun.* **16**, 332 (2025).
35. Sudhakar, P., Gupta, A. K., Cordes, D. B. & Zysman-Colman, E. Thermally activated delayed fluorescence emitters showing wide-range near-infrared piezochromism and their use in deep-red OLEDs. *Chem. Sci.* **15**, 545–554 (2024).
36. Li, G., Tian, Y., Zhao, Y. & Lin, J. Recent progress in luminescence tuning of Ce^{3+} and Eu^{2+}-activated phosphors for pc-WLEDs. *Chem. Soc. Rev.* **44**, 8688–8713 (2015).

37. Dorenbos, P. Lanthanide 4*f*-electron binding energies and the nephelauxetic effect in wide band gap compounds. *J. Lumin.* **136**, 122–129 (2013).

38. Zhang, H., Zhang, J., Ye, R., Xu, S. & Bai, G. Color modulation of cerium sulfide colorant powders through chemical doping engineering. *J. Mater. Chem. C.* **11**, 9215–9222 (2023).

39. Zhang, H. et al. Impurity doping effects and ecological friendly synthesis of cerium sulfide powders for enhanced chromaticity and color tunability. *Ceram. Int.* **49**, 34090–34096 (2023).

40. Borkovec, A. B., Oliver, J. E., Chang, S. C. & Brown, R. T. Insect chemosterilants. 10. Substituted dithiobiurets. *J. Med. Chem.* **14**, 772–773 (1971).

41. Bêche, E., Charvin, P., Perarnau, D., Abanades, S. & Flamant, G. Ce 3d XPS investigation of cerium oxides and mixed cerium oxide ($Ce_xTi_yO_z$). *Surf. Interface Anal.* **40**, 264–267 (2008).

42. Dorenbos, P. 5*d*-level energies of Ce^{3+} and the crystalline environment. III. Oxides containing ionic complexes. *Phys. Rev. B* **64**, 125117 (2001).

43. Wei, Y., Dang, P., Dai, Z., Li, G. & Lin, J. Advances in near-infrared luminescent materials without Cr^{3+}: Crystal structure design, luminescence properties, and applications. *Chem. Mater.* **33**, 5496–5526 (2021).

44. Guo, R. et al. Luminescent rare earth complexes of Ce^{3+}, Eu^{2+} and Yb^{2+} with spiro-bis(pyrazolyl)borate ligands containing C–H···M interactions. *J. Rare Earths* (2024).

45. Amachraa, M. et al. Predicting thermal quenching in inorganic phosphors. *Chem. Mater.* **32**, 6256–6265 (2020).

46. Qi, H. et al. Air stable and efficient rare earth Eu (II) hydro-tris (pyrazolyl) borate complexes with tunable emission colors. *Inorg. Chem. Front.* **7**, 4593–4599 (2020).

47. Aguirre Quintana, L. M., Jiang, N., Bacsa, J. & La Pierre, H. S. Homoleptic cerium tris(dialkylamido)imidophosphorane guanidinate complexes. *Dalton Trans.* **49**, 14908–14913 (2020).

48. Harris, K. R., Malhotra, R. & Woolf, L. A. Temperature and density dependence of the viscosity of octane and toluene. *J. Chem. Eng. Data* **42**, 1254–1260 (1997).

49. Santos, F. J. V. et al. Standard reference data for the viscosity of toluene. *J. Phys. Chem. Ref. Data* **35**, 1–8 (2005).

50. Dolomanov, O. V., Bourhis, L. J., Gildea, R. J., Howard, J. A. K. & Puschmann, H. OLEX2: a complete structure solution, refinement and analysis program. *J. Appl. Crystallogr.* **42**, 339–341 (2009).

51. Macrae, C. F. et al. Mercury 4.0: from visualization to analysis, design and prediction. *J. Appl. Crystallogr.* **53**, 226–235 (2020).

Acknowledgements

Author contributions

Jiayin Zheng conducted most of the experiments and wrote the manuscript. Haodi Niu conducted the synthesis of the organic intermediates and measurement of the FT-IR data. Ruoyao Guo and Yujia Li measured the PLQY values. Haodi Niu, Huanyu Liu, Wen Lu, Tianming Zhong, Zuqiang Bian, and Zhiwei Liu revised the manuscript and provided suggestions. All authors discussed the results and contributed to the paper.

Competing interests

The authors declare no competing interests.

Additional information

Supplementary information The online version contains supplementary material available at https://doi.org/10.1038/s41467-025-63226-3.

Correspondence and requests for materials should be addressed to Zhiwei Liu.

Peer review information *Nature Communications* thanks Feng Liu and the other anonymous reviewer(s) for their contribution to the peer review of this work. A peer review file is available.

Reprints and permissions information is available at http://www.nature.com/reprints

Publisher's note Springer Nature remains neutral with regard to jurisdictional claims in published maps and institutional affiliations.